Regenerative Medicine

Delivery of hepatocyte growth factor mRNA from nanofibrillar scaffolds in a pig model of peripheral arterial disease

Tatiana S Zaitseva[‡,1], Guang Yang[‡,2,3], Dimitris Dionyssiou[1,4], Maedeh Zamani[2,5], Steve Sawamura[1], Eduard Yakubov[6], James Ferguson[7], Richard L Hallett[2,8], Dominik Fleischmann[2,8], Michael V Paukshto[1] & Ngan F Huang*[,2,3,5] (iD)

[1]Fibralign Corporation, Union City, CA 94587, USA
[2]Stanford Cardiovascular Institute, Stanford, CA 94305, USA
[3]Veterans Affairs Palo Alto Health Care System, Palo Alto, CA 94304, USA
[4]Department of Plastic Surgery, Aristotle University of Thessaloniki, Thessaloniki 54124, Greece
[5]Department of Cardiothoracic Surgery, Stanford University, Stanford, CA 94305, USA
[6]PhaRNA, LLC, Houston, TX 77024, USA
[7]Palo Alto Bioresources, Berkeley, CA 94705, USA
[8]Department of Radiology, Stanford University, Stanford, CA 94305, USA
*Author for correspondence: Tel.: +650 849 0559; ngantina@stanford.edu
[‡]Authors contributed equally

Background: Chemical modification of mRNA (mmRNA) substantially improves their stability and translational efficiency within cells. Nanofibrillar collagen scaffolds were previously shown to enable the spatially localized delivery and temporally controlled release of mmRNA encoding HGF both *in vitro* and *in vivo*. **Materials & methods:** Herein we developed an improved slow-releasing HGF mmRNA scaffold and tested its therapeutic efficacy in a porcine model of peripheral arterial disease. **Results & conclusion:** The HGF mmRNA was released from scaffolds in a temporally controlled fashion *in vitro* with preserved transfection activity. The mmRNA scaffolds improved vascular regeneration when sutured to the ligated porcine femoral artery. These studies validate the therapeutic potential of HGF mmRNA delivery from nanofibrillar scaffolds for treatment of peripheral arterial disease.

Poor vascularization and the ensuing tissue ischemia complicate the outcome of many diseases including critical limb ischemia [1,2]. A promising strategy to improve vascular growth is to induce therapeutic angiogenesis, arteriogenesis and lymphangiogenesis, by targeting the production of key vascular growth factors [3–5]. Gene therapy is a powerful approach to regulate target protein expression for regenerative applications [6]. Most commonly, it employs DNA-based viral or plasmid vectors [7,8]. DNA viral vectors include the possibility of viral integration into the host genome, immunogenicity and gene silencing [9]. Plasmid DNA vectors have reduced immunogenicity and risk of genome integration [10–12] but are generally much less efficient in protein production [13–16]. These disadvantages present a concern for clinical applications.

Synthetic modified mRNA is a nonviral RNA-based technology that solves many of the safety concerns [17]. In particular, advantages of modified mRNA-based vector delivery over conventional plasmid or viral-based technologies include: negligible risk of genome integration or insertional mutagenesis [18]; absence of gene silencing due to independence of promoter activity and; faster and more efficient modulation of target protein expression [19]; similar efficiency of mRNA-mediated expression in both mitotic and postmitotic cells [20]. Despite these advantages, modified mRNA vectors have been much less widely used partly due to technical challenges in synthesizing nonimmunogenic mRNA vectors [13]. Recent progress in developing chemically modified mRNA (mmRNA) by incorporation of nucleotide analogs have shown substantially improved intracellular stability and translational efficiency while obviating innate immunity activation [14,21]. Intracellular delivery of mRNA has been facilitated

Future Medicine

Regen. Med. (2020) 15(6), 1761–1773

by complexation with a transfection agent, with RNA encapsulation into lipid nanoparticles being one of the most developed delivery methods [22]. With these advances, mmRNA therapy has already shown promising therapeutic benefits to treat a number of diseases [14,23–25], in particular vascular regeneration by angiogenic VEGF mmRNA [26].

The wider adoption of mmRNA therapy for site-specific clinical use may also be limited by predominantly solution-based delivery mode used for soft tissue regeneration [27–29]. Delivery of genetic material in solution shows dependency on injection technique [30] and variability in protein expression within [26,28,31] and systemic spread beyond [32] specific target area. Unlike delivery in solution, biomaterials-based delivery of genetic cargo targets cell populations located in the vicinity of the scaffold [33], enables controlled release of the cargo [34], and obviates premature clearance associated with solution-based delivery [35]. Scaffold-based delivery of mmRNA has been proven effective for bone regeneration [36–38].

In our recent studies, we developed a technology using parallel-aligned nanofibrillar scaffolds for spatially controlled and transient release of mmRNA. We have based our rationale on the potential synergy between the two components of the device. First, the transient delivery of therapeutic mmRNA encoding angiogenic factors such as HGF may be suitable for inducing angiogenesis without malformations observed after long-term uncontrolled expression of angiogenic transgenes [39]. Second, a 3D scaffold intended for mmRNA delivery may also provide the structural framework for cellular recruitment and tissue formation in response to mmRNAs that encode angiogenic factors. Since physiological extracellular matrix is mainly composed of nano- to micro-scale fibrillar networks [40], we previously engineered aligned braided nanopatterned collagen scaffolds that induce cellular reorganization of the cytoskeleton along the direction of the nanofibrils [41–43], and improved cell survival [44,45]. Along with other studies which demonstrated a role of nanofibrillar cues in modulating cell function, stem cell differentiation, cellular reprogramming and tissue morphogenesis [46–48], this body of data suggest that nanofibrillar scaffolds modulate basic cellular processes. Of note, these nanofibrillar scaffolds have been shown to enhance angiogenesis [49], arteriogenesis [50] and lymphangiogenesis [51] *in vivo*. We have further shown therapeutic benefit of HGF mmRNA-releasing scaffolds, by demonstrating enhanced vascular regeneration after their implantation in the injured skeletal muscle [52].

In this study, we developed an improved slow-releasing HGF mmRNA scaffold and demonstrated its therapeutic efficacy in a porcine model of peripheral arterial disease (PAD). The HGF mmRNA was released from mmRNA-loaded scaffolds in a transient and temporally controlled fashion for up to 4 weeks *in vitro*. When fibroblasts were seeded onto the HGF mmRNA-releasing scaffolds, the cells demonstrated induced secretion of HGF protein for up to 4 weeks *in vitro*. Initial studies of scaffold-based delivery of HGF mmRNA to the site of the ligated femoral artery in six pigs resulted in increased vascularity at 5 weeks postimplantation, relative to that of the contralateral limb that received no treatment, based on computed tomography (CT) imaging. This finding was supported by hematoxylin and eosin (H&E) staining of tissue sections adjacent to the site of scaffold implantation, showing the presence of arterioles near the site of scaffold implantation. Furthermore, quantification of capillary density within the vicinity of the implanted scaffold demonstrated marked increase in vascular regeneration, compared with surrounding tissue, suggesting a treatment-mediated angiogenic effect. These studies demonstrate a promising therapeutic approach for the delivery of HGF mmRNA from nanofibrillar scaffolds for treatment of PAD.

Materials & methods
Fabrication of aligned nanofibrillar scaffolds
The aligned nanofibrillar collagen scaffolds were fabricated using shear-based fibrillogenesis technique, crosslinked by 1-ethyl-3-(3-dimethylaminopropyl)-1-carbodiimide hydrochloride (EDC) chemistry and sterilized by e-beam per standard protocols (Fibralign Corporation, CA, USA) as described previously [45].

Preparation of mmRNA-loaded scaffolds
mmRNA encoding human HGF were provided by PhaRNA, LLC (TX, USA). HGF mmRNA was synthesized using predesigned and linearized plasmid templates. The mmRNA was modified by the replacement of uridine with pseudouridine and cytidine with 5-methylcytidine, post-transcriptional incorporation of Cap1 structure, and an addition of a constant extralong stabilizing poly-A tail (175 nucleotides long). A loading mixture was prepared from mmRNA combined with Lipofectamine MessengerMax transfection agent (Invitrogen, CA, USA), 22 mg/ml sucrose and 0.15 mg/ml collagen used in aligned nanofibrillar scaffold production. For *in vitro* studies of RNA release and transfection, 450 ng mmRNA was loaded into the 5 mm scaffold nanofibrillar scaffolds, as described previously. For *in vivo* studies, the scaffold construct was scaled up as follows (Figure 1). The loading mmRNA
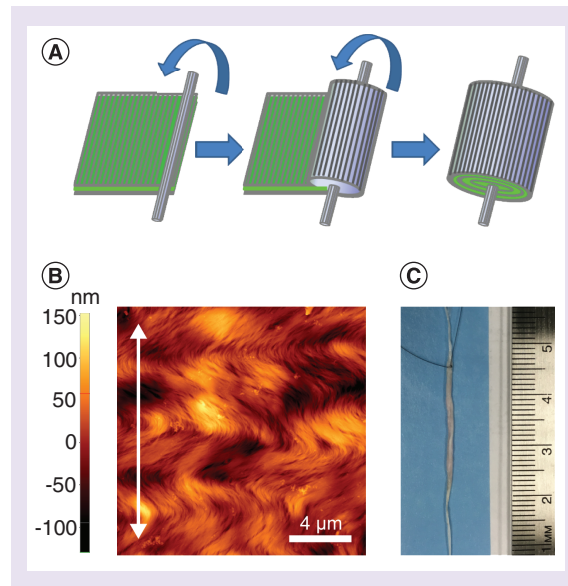
Figure 1. Scaffold fabrication and characterization. (A) To fabricate the mmRNA-releasing scaffold, the HGF mmRNA cocktail was sandwiched between two 2 μm layers of aligned collagen matrix (25 × 25 mm) and then lyophilized. Next, the resultant collagen/mmRNA sandwich was rolled around 6 cm section of a thread-like nanofibrillar scaffold, and finally tagged with a 6–0 suture to facilitate the positioning of the scaffold. **(B)** Characterization of dimensions and topography of aligned nanofibrillar collagen matrix by atomic force microscopy. **(C)** Gross morphology of HGF mmRNA-releasing scaffold. Scale bar: 4 μm.

mixture was sandwiched between two 2 μm layers of aligned collagen matrix (25 × 25 mm) and lyophilized. The resultant collagen envelope with mmRNA material was rolled around 6 cm section of a regular nanofibrillar scaffold, and tagged with a 6–0 suture to facilitate the positioning of the scaffold (Figure 1). For *in vivo* studies, 100 μg of mmRNA was loaded into each scaffold. All procedures were performed under sterile conditions.

Kinetics of mmRNA release *in vitro*

The kinetics of GFP-encoding mmRNA release were quantitatively assessed using the Quant-iT Ribogreen quantification kit (Life Technologies, OR, USA) according to the manufacturer's instructions. The mmRNA-loaded scaffolds were incubated in 100 μl TE buffer containing 10 mM Tris-HCl and 1 mM EDTA (TE buffer, pH 7.5). At specified time points, the conditioned TE buffer was collected for quantification by Ribogreen assay, and replaced with fresh TE buffer. After 30 days, the scaffolds were digested with proteinase K, and the mmRNA released from the scaffolds was quantified as described above to obtain the total recovered mmRNA per scaffold (n = 3).

Transfection with HGF mmRNA *in vitro*

Human fibroblasts (SCRC1041, ATCC, passages 5–10) were expanded in DMEM with 10% fetal bovine serum and 1% penicillin/streptomycin. HGF mmRNA-loaded scaffolds were placed into 96-well ultra-low attachment plate, and seeded with 1×10^5 fibroblasts for 2 h. Next, the media with unattached cells were removed and replaced with fresh media. Cells were cultured on scaffolds for indicated time intervals (n = 3). For HGF mmRNA-transfected cells, aliquots of media were collected periodically for analysis of secreted HGF protein and replaced with fresh media.

ELISA

HGF concentration in media samples was measured by HGF ELISA kit (R&D Systems, MN, USA) following manufacturer's instructions (n = 3).

Hindlimb ischemia model

All animal experiments were performed with approval by the Institutional Animal Care and Use Committee at the Sutter Institute of Medical Research (CA, USA). Hindlimb ischemia in Yorkshire pigs (n = 6, 30 ± 5 kg) was induced following a previously described protocol [53]. After induction of anesthesia with Telazol (3–8 mg/kg, intramuscularly [IM]) and mask-administered isoflurane gas (1–4%), animals were intubated and anesthesia was maintained with isoflurane (1–4%) combined with 100% oxygen using mechanical ventilator (Hallowell Model 2002 Veterinary Anesthesia Ventilator). Upon anesthetic induction, animals received Cefazolin (22 mg/kg, intravenously [IV]). Respiration and electrocardiography were continuously monitored during each imaging session.

An 18G IV catheter was placed for the administration of fluids and CT contrast agent. Animals were injected with CT contrast agent and images of the intact vasculature were acquired. Under standard surgical sterile procedures, both the right and left superficial femoral artery were isolated and two ligations, approximately 2.5 cm apart, were placed proximal to the deep femoral artery. Immediately after the artery ligation, two scaffolds were placed in the right hind limb parallel to the ligated right superficial femoral artery. The left superficial femoral artery of each pig was also ligated but did not receive an implant. The scaffolds were secured by microclips or 8–0 prolene sutures to the ligated femoral artery, followed by suture closing the skin. The femoral sites were closed in a standard three-layer closure. Animals were given ketoprofen (1–3 mg/kg IM) and buprenorphine (0.005–0.01 mg/kg IM) for analgesia. CT imaging was performed immediately after ligation of the arteries; 2 and 5 weeks after implantation, followed by postmortem angiography. Animals were euthanized with 20–40 mEq KCl while being maintained under deep anesthesia. Euthanasia was verified via electrocardiography, lack of respiration and loss of reflexes.

CT angiography
Intravital CT images were obtained at baseline, immediately after occlusion; 2 and 5 weeks after occlusion. A 64-slice CT scanner (Lightspeed, GE Healthcare, IL, USA) and iodinated contrast (300 mgI/ml, Omnipaque, GE Healthcare, IL, USA) were used. Images were obtained at a slice thickness of 0.6 mm, at 300 mA and 120 kVp. Contrast solution was delivered intravenously with a power injector (Stellant D, MEDRAD, Bayer Medical Care, PA, USA) at a constant rate of 3 ml/s and total volume of 30 ml, followed by a 0.9% sodium chloride injection at 3 ml/s, and the images were acquired as described above. Commercially available software (AquariusNet, TeraRecon Inc., CA, USA) was used for manual bone segmentation and reconstruction of 3D images.

Postmortem CT angiography
At the end of experiment, 64-slice CT angiography (Lightspeed, GE Healthcare) was performed after the casting of hindlimb vasculature to improve visualization of small vessels and confirm the presence of new collateral vessels as described [53]. Prior to euthanization, animals received 3 ml of heparin (1000 IU/l) intravenously. After euthanization, the abdominal aorta was cannulated and the vasculature was rinsed with 0.9% sodium chloride injection. Contrast agent containing 15% bismuth (Sigma-Aldrich, MO, USA) in 10% gelatin, approximately 50–150 ml, was then injected manually, and the images were acquired and processed in the same way as for intravital CT.

Tissue sample harvesting
At the end of experiment, animals were euthanized, and tissue samples were harvested from the implantation or artery ligation only areas. Following immediate fixation in 10% buffered formalin, samples were dehydrated in a gradient of ethanol solution, embedded in paraffin and 6 μm transverse sections were made by microtome for routine H&E evaluation.

Histology & analysis of microvascular density
The paraffin-embedded tissue sections were first de-paraffinized using Safeclear II (xylene substitute) and rehydrated with graded ethanol solutions and then routine H&E staining was performed. The H&E stained tissues were brightfield imaged using a Keyence microscope (BZ-X700, Osaka, Japan) at 10×, by XY-stitching of 7 × 9 multi-tile images captured from the surrounding area of the scaffold. For immunofluorescence staining of blood vessels in paraffin-embedded tissue sections, antigen retrieval was carried out on rehydrated sections at high heat using IHC Antigen Retrieval Solution-Low pH (ThermoFisher Scientific, MA, USA) at 1×. Then, tissue sections were incubated with vascular smooth muscle marker α-SMA antibodies (Sigma-Aldrich, MO, USA) followed by incubation with Alexafluor-488-conjμgated secondary antibody (Life Technologies, CA, USA). Finally, the nuclei were visualized using Hoechst 33342 dye (Life Technologies). The immunofluorescently stained tissues were imaged using a fluorescence microscope (BZ-X700, Keyence, Osaka, Japan) at 10×, by XY-stitching of 7 × 9 images captured from surrounding area of the scaffold. This procedure was developed and successfully applied in our previous study [51].

Quantification of blood vessel regeneration
For quantification of microvasculature density within vicinity of the scaffolds, regional rings were drawn at radial distances of 0–50, 51–100, 101–150, 151–200 and 201–1000 μm surrounding the periphery of the scaffold using
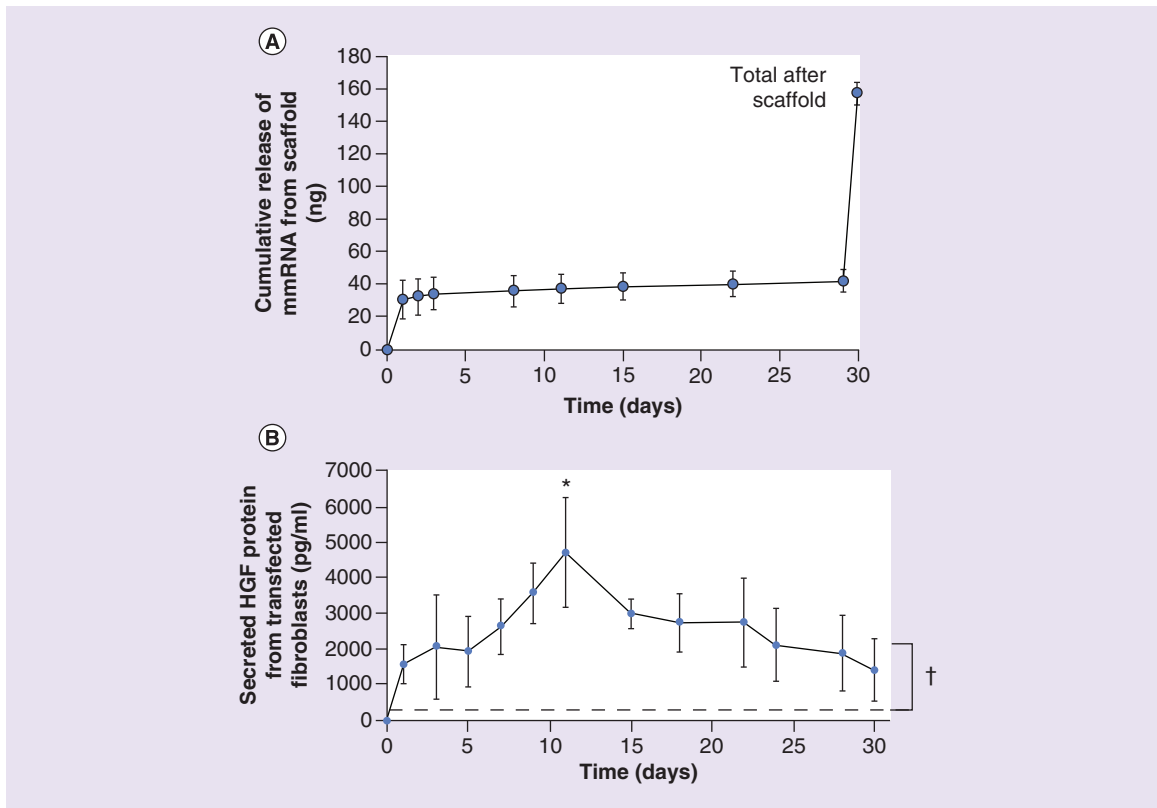
Figure 2. Characterization of HGF mmRNA release and HGF protein release *in vitro*. (A) Cumulative mmRNA release from HGF mmRNA-loaded aligned nanofibrillar scaffold (n = 3). **(B)** HGF concentration in media from fibroblasts cultured on HGF mRNA-loaded scaffold, quantified by HGF ELISA (n = 4). Dotted line denotes the highest detectable level of endogenous HGF in control samples. *Denotes statistically significant relationship, compared with day 0 (p < 0.05).
†Statistically significant compared with endogenous HGF protein concentration in control samples (p < 0.05).

ImageJ software (US NIH, MD, USA), based on the established methods from our previous publication [51]. Within each ring, the number of blood vessels (α-SMA-positive) were counted and expressed in the form of density (#/mm^2) by normalizing to the area of each individual ring. As the control for vascular regeneration effects of the scaffold, microvasculature densities were also quantified for tissue regions >1000 μm away from the scaffolds.

Statistical analysis

All data are shown as mean ± standard deviation. Statistical comparisons between two groups were quantified by an unpaired t-test. For comparisons of three or more groups, analysis of variance with Holm's adjustment for multiple comparisons was used. Statistical significance was accepted at p < 0.05.

Results

Verification of mmRNA release & transfection for HGF mmRNA-loaded scaffold

Evaluation of mmRNA release profile from the scaffolds loaded with 450 ng mmRNA demonstrated a sustained release of RNA (Figure 2A), with ~22% loaded RNA released during the first day of incubation in TE buffer, followed by slow release during the 30-day experiment, and 73% loaded RNA remaining in the scaffold on day 30. These HGF mmRNA-loaded scaffolds showed an average load recovery of 34.9 ± 6.2% (as compared with the nominal amount of RNA loaded). Next, scaffolds loaded with 450 ng HGF mmRNA were seeded with fibroblasts, and HGF protein secreted into media was measured by HGF ELISA. The results show that HGF concentration in cell culture media reached the peak on day 11 at 4707 pg/ml, and was sustained through the 30-day culture period (Figure 2B). For comparison, endogenous HGF secretion by cells grown on tissue culture plastic did not exceed 383 pg/ml.
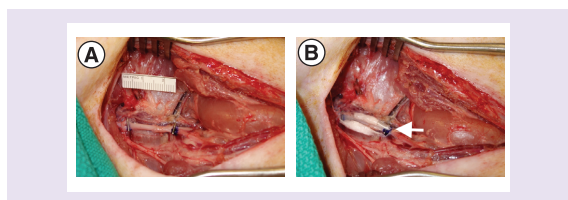
Figure 3. Implantation of HGF mmRNA-loaded scaffolds into a porcine model of peripheral arterial disease. (A) Gross morphology of femoral artery ligation. **(B)** Implantation of HGF-RNA loaded scaffolds along the ligated artery. Arrow shows the scaffolds secured to the artery.
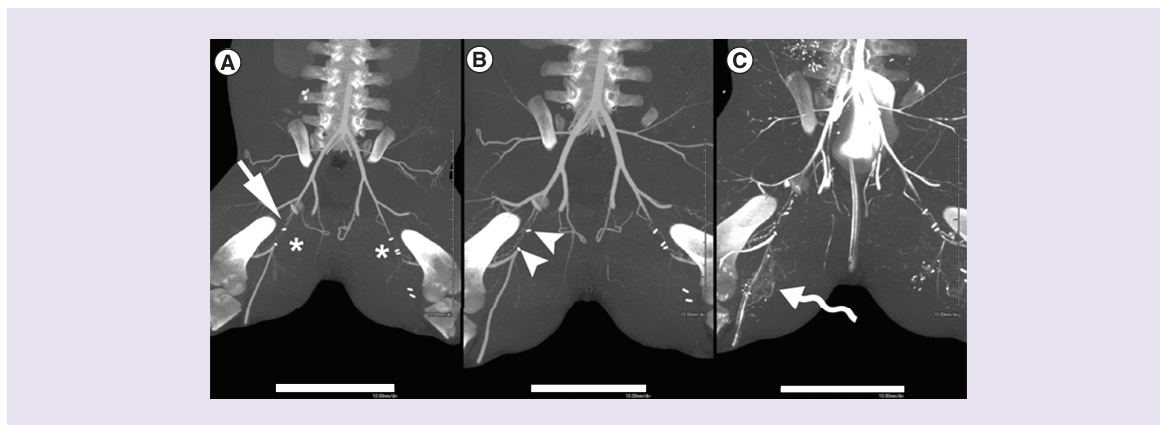

Figure 4. Computed tomography angiograms depict microvascular formation in the ischemic porcine limb after treatment with HGF mmRNA-releasing scaffold. CTA imaging was performed at 2 weeks **(A)** and at 5 weeks **(B & C)**. A 5-week CTA was performed with iodinated contrast medium **(B)** and with bismuth injection postmortem **(C)**. In **(A)**, note the ligated vascular segments on both sides (*). On the treated right side **(straight arrow)**, early and asymmetric neovascularity can be demonstrated. By 5 weeks **(B)**, visualized serpentine collateral channels have become more prominent and more pronounced **(arrowheads)** compared with the nontreated side. Injection of bismuth **(C)** to fully distend all vascular channels shows even more prominent vascularity on the right **(curved arrow)**. Scale bar: 10 cm. CT: Computed tomography; CTA: CT angiogram.

Scaffold preparation & implantation in ischemia model

Having verified the transfection efficiency of RNA-loaded scaffold *in vitro*, the length of the RNA-loaded construct were increased to 2.5 cm to cover the ligated section of the femoral artery in pig ischemia model (Figure 3A). Based on the previous studies suggesting that mmRNA loading suitable for *in vivo* transfection range between 10 and100 μg [29], and our earlier studies demonstrated the efficiency of 20 μg RNA load in mice [52], a total of 200 μg RNA was selected for delivery per injury site. Two scaffolds were implanted per site, each loaded with 100 μg RNA. After the right femoral artery was ligated, the scaffolds were placed along the ligated section and secured with microclips or 8–0 prolene sutures to the ligated artery section (Figure 3B).

Intravital CT angiography

CT images were acquired prior and immediately after ligation of the femoral arteries to identify the impaired blood flow at the site of ligation. CT images taken at 2 weeks after implantation demonstrated early and asymmetric neovascularity at the site of implantation (Figure 4A). CT images obtained 5 weeks after implantation of the HGF-RNA loaded scaffold revealed serpentine collateral channels which had become more prominent and more pronounced (arrowheads) compared with the nontreated side (Figure 4B). This type of collateral formation was found in 2 of 6 pigs examined at 5 weeks postimplantation.

Postmortem angiography

Postmortem CT angiography improved the image quality of the vasculature obtained by intravital CT and verified new collateral formation. Detailed image analysis showed that at 5 weeks postimplantation, in addition to serpentine collateral channels at the site of implantation, more prominent vascularity was seen distally from the implantation site (Figure 4C, curved arrow), as compared with the untreated left side.

Figure 5.   Histological analysis of the femoral artery occlusion site at 5 weeks after implantation of an HGF mmRNA-releasing scaffold. (A) H&E stained image of the scaffold-treated right hindlimb depicts the presence of small collateral arterioles **(denoted by *)** and interfascicular neural arterioles **(denoted by arrow).** **(B)** The contralateral left hindlimb **(untreated)** show interfascicular neural arterioles **(denoted by arrows).** Scale bar denotes 1 mm.
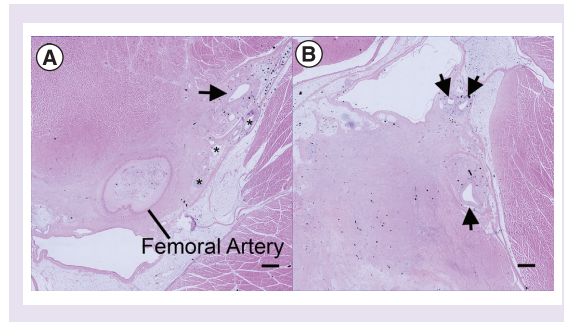H&E: Hematoxylin and eosin.

Figure 6.   Histological analysis of microvascular density. **(A)** H&E staining of the implantation site with occluded FA and scaffold. Dotted circle denotes location of scaffold. **(B)** Corresponding tissue section immunofluorescently stained for microvessels using α-SMA antibody. **(C)** Quantification of relative percent change in microvascular density in the vicinity of HGF mmRNA-releasing scaffold, compared with surrounding tissue >1000 μm in radial distance away from the scaffold (n = 3). Dotted line denotes the relative microvascular density in the surrounding tissue. Scale bar denotes 1 mm.
*Denotes statistically significant difference in comparison to surrounding tissue ($p < 0.05$).
FA: Femoral artery; H&E: Hematoxylin and eosin.
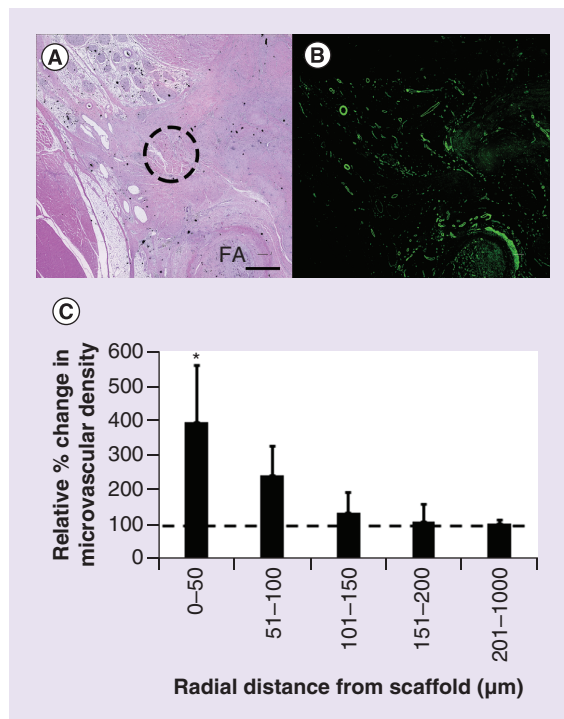
Histological evaluation of remodeling & revascularization

Analysis of H&E sections revealed the obvious presence of implanted scaffold in three of six animals (Figure 5). In the other three animals, although remnants of the scaffold material could be observed, the scaffold was probably quite extensively remodeled, so it was not possible to accurately determine the exact implantation site. Therefore, we proceeded with analysis of microvascular density in the specimens where scaffold was present.

Quantification of microvasculature density within vicinity of the scaffolds demonstrated the formation of neovessels around the scaffold (Figure 6). Our data showed that microvascular density within the vicinity of the scaffold increased by fourfold, relative to the surrounding tissue (Figure 6C). The spatiotemporally regulated improvement in angiogenesis suggested that the improvement was a result of localized mmRNA release and subsequent angiogenic response.

The results of this study support our hypothesis that the HGF-activated nanofibrillar scaffold would: promote cell attachment to and elongation along the nanofibrils and; provide HGF vector delivery to the attached cells with high transfection efficiency (due to cell elongation on nanofibrils); induce secretion of HGF by cells along the thread; and attract endothelial cells and endothelial progenitor cells (EPC) to form vascular networks along the direction of the nanofibrils (Figure 7). This approach is intended to improve the recruitment of endogenous endothelial cells and EPC toward the scaffold, as well as to guide the spatial orientation of newly formed vessels using the scaffold's nanostructure. Our concept is in line with previous studies, where the authors enhanced cardiac regeneration using 3D fibrous PLLA mats loaded with VEGF protein and preseeded with cardiac stem cells [54].
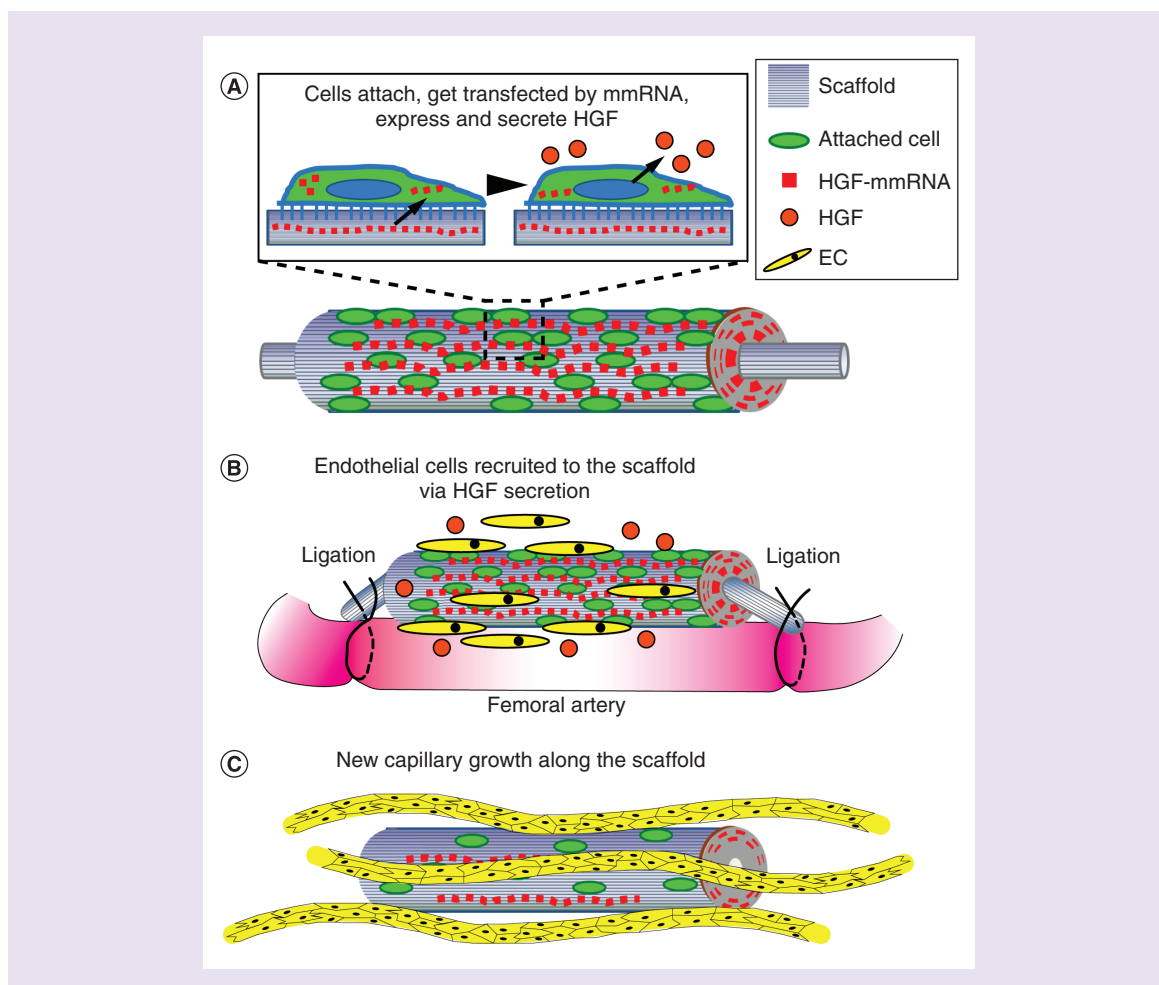
Figure 7.   Suggested steps following implantation of scaffold loaded with HGF vector. (A) In the presence of the aligned collagen, a number of cells attracted to ischemic region attach to the scaffold, get transfected and produce HGF. **(B)** Secreted HGF attracts more cells, including local endothelial and endothelial precursor cells. **(C)** Endothelial cells migrated to the scaffold eventually form new capillaries along the scaffold.
EC: Endothelial cell.

Discussion

In recent years, mmRNA-based therapy has become a promising approach due to the negligible risk of mmRNA mode of expression, natural biodegradation pathways and efficiency of translation of the encoded therapeutic protein directly by translational machinery of mammalian cells. The clinical translation of mmRNA therapeutics has been made possible through advances in the design of mRNA manufacturing and intracellular delivery methods. However, broad application of mRNA is still limited by the need for improved delivery systems.

Using a biomaterials-based delivery approach, we showed that mmRNA release and cellular transfection can be successfully achieved using aligned nanofibrillar collagen scaffolds. The salient findings from this study are as follows: first, HGF mmRNA was released from mmRNA-loaded scaffolds in a transient and temporally controlled fashion for up to 4 weeks *in vitro*; second, human fibroblasts seeded onto the HGF mmRNA-releasing scaffolds maintained secretion of HGF protein for up to 4 weeks *in vitro*; third, implantation of HGF mmRNA-releasing scaffolds into the site of the ligated femoral artery in five pigs resulted in increased vascularity at 4 weeks postimplantation, relative to that of the contralateral limb that received no treatment, based on CT imaging; fourth, the presence of arterioles was shown by hematoxylin and eosin staining of tissue sections adjacent to the site of scaffold implantation; and finally, quantification of capillary density within the vicinity of the implanted scaffold demonstrated marked increase in vascular regeneration, compared with surrounding tissue and suggested a treatment-mediated angiogenic effect.

Preparation of the scaffold for implantation in large animal model involved scaling up the dimensions and the RNA load we used previously in a small animal study. Considering the longer timeline of experiment in pig model, we modified the formulation of RNA mix, adding collagen to the final composition to slow down the release of RNA. The use of collagen has previously been used in DNA delivery [55]. Addition of collagen reduced the initial burst of RNA release compared with previous formulation [52]. RNA was released from the scaffold for over 4 weeks, and at this time point scaffold still retained 73% of total recovered RNA load. Accordingly, the levels of HGF secreted into media by fibroblasts transfected after seeding onto the HGF mmRNA-releasing scaffolds were maintained for a longer period of time.

The mmRNA appeared to have undergone partial degradation in the aligned collagen scaffolds, with the amount of RNA recovered from the freshly loaded scaffolds measured as 62% of initial nominal load. There was apparent degradation during the leaching experiment *in vitro*, based on reduction of total RNA recovery (35% of initial nominal load) after a month-long leaching experiment. The potential reasons could be due to the stability of mmRNA in the presence of naturally-derived biomaterials like purified collagen which could contain trace amounts of RNAses or other enzymes. Another contributing factor to the degradation of mmRNA could be the negative pressure associated with the freeze drying step for incorporating mmRNA into the scaffold. Despite partial degradation of the mmRNA in the nanofibrillar scaffolds and its slow-release profile demonstrated in the leaching experiment, we confirmed that the mmRNA could successfully transfect cells *in vitro* with maintaining HGF secretion by fibroblasts for over 4 weeks.

In our previous studies, 20 µg of HGF mmRNA delivered on the scaffold showed a therapeutic effect. In this study, a therapeutic effect was achieved with 200 µg total amount of HGF mmRNA delivered by two scaffolds in porcine hindlimb ischemia model. Higher doses of VEGF mmRNA were reported to improve myocardial function in pigs when delivered by injection in sucrose citrate buffer at 1–10 mg [56]. In comparison, injection of 4 mg HGF DNA in chronic porcine myocardial ischemia model significantly reduced ischemic area, increased capillary density and regional myocardial perfusion in the ischemic area. Much lower doses of mmRNA (72 µg) formulated into lipid nanoparticles, injected in the pig heart, were able to induce expression of GFP [57], suggesting that transfection agents may improve translation efficiency. One measure of translation efficiency is the ratio of therapeutic mmRNA dose to bodyweight. In our study, this number is 0.007 µg/g (for 200 µg RNA per 30 kg average weight pig, and comparable with 0.009 in the study where BMP mmRNA-loaded collagen scaffold was used for bone repair in rat (2.5 µg per 285 g average weight rat [38]). To the best of our knowledge, none of the mmRNA formulations delivered by injection achieved this efficiency [26,56,58]. Comparison of dose efficiencies is complicated due to different models used to evaluate RNA therapy. Severity of the disease may affect translation, as suggested by threefold lower GFP levels after intracoronary GFP mRNA injection 48 h after myocardial infarction [56].

Compared with conventional systemic delivery approaches, mmRNA release from scaffold enables localized delivery and controlled release of the transcript at higher concentration, and thus, a lower amount of mRNA may be required to exert therapeutic effect in the target tissue [38]. The sustained yet temporal release of mRNA transcript can also prevent inappropriately high expression of the encoding protein, resulting in lower risk of abnormal tissue formation reported for DNA vectors [59]. However, the temporal release profile from this study was likely dependent on the initial concentration. Additionally, the morphology and physicochemical properties of the scaffold play a significant role in determining transfection efficiency of mRNA [60]. Natural tissue development is a complex process that requires spatial and temporal arrangement of expression of different types of proteins, signaling molecules and matrix molecules in the cellular environment. Having mRNA incorporated into the aligned scaffold may approximate the spatial patterns in target protein expression by the cells attached to the scaffold, which can potentially direct the tissue formation and development of spatially patterned structures such as blood vessels [61,62].

Fabrication of mRNA-loaded scaffold using nonspecific adsorption of mRNA to the scaffold followed by a simple final assembly minimizes the risk of mRNA degradation and allows for the mRNA being distributed throughout the scaffold. The presence of mRNA on the surface facilitates the early cellular uptake by the cells attached to the substrate. Along with layer-by-layer biodegradation of the scaffold material, more mRNA is released and becomes available for transfection. The scaffold material can modulate transfection efficiency not only through regulating cell adhesion and subsequent transfection, but also by determining the cell internalization pathway of the gene complex [63]. Importantly, making the scaffold from atelocollagen [55] can minimize the inflammatory responses, and subsequently reduce mRNA degradation and elimination of the transfected cells [64].

Having shown a therapeutic effect of HGF mmRNA releasing scaffold in a clinically relevant model, we envision that scaffold-based delivery of mmRNA may be applied for treatment of a variety of diseases, including those of

the cardiovascular, nervous and musculoskeletal systems. For example, for treatment of PAD that is characterized by vascular obstructions in the limbs, the scaffold loaded with mmRNA encoding angiogenic factors could be transplanted to the skeletal muscle adjacent to the vascular obstruction to allow for transient growth factor delivery to augment neovascularization. The findings from this work have important implications in the design of gene therapy for soft tissue regeneration.

Limitations

One limitation of the study is small sample size. Though we were able to show therapeutic effect with the current dose, expanding the study to investigate a wider range of RNA doses also would be beneficial. Furthermore, other porcine surgical models of PAD that induce a more severe limb ischemia [65] should be considered to better represent the pathobiology of PAD patients.

Conclusion

Together, we developed nanofibrillar scaffold system that enables prolonged-delivery of HGF-encoding mmRNA in this study. Our *in vitro* findings substantiate that mmRNA can be successfully delivered from scaffolds to transfect seeded fibroblasts. Moreover, we noted an *in vivo* functional effect of our scaffold in terms of the therapeutic angiogenesis and blood flow restoration in a clinically relevant pig injury model. Our study represents a promising novel therapeutic approach for the treatment of PAD.

Translational perspective

Gene therapy applications for treatment of PAD and its more severe form, critical limb ischemia, have been recently investigated in many preclinical and clinical studies. It employs genetic material encoding for therapeutic proteins that may help induce revascularization when delivered to the diseased limb. So far, clinical studies have shown the safety of gene therapy in limb ischemia. However, the therapeutic effect was largely limited to improved complete ulcer healing, and no clear reductions in amputation-free survival, major amputation and all-cause mortality were achieved. More effective gene therapy may include expanding nucleic acid vectors to mRNA, and combining it with new scaffold delivery methods. Preclinically, tailored devices for mRNA delivery have been proven to be efficient in bone regeneration. Using specific scaffolds for vascular regeneration immediately provides relevant environment for endothelial cells. Furthermore, providing a tissue-specific scaffold to deliver mRNA holds the key to high translatability of the encoded therapeutic protein. New treatments may benefit from delivering two or more vectors from one scaffold, and combinations may include mRNA-releasing scaffold with stem cells. Further studies are needed to develop new treatment options able to achieve revascularization in patients with PAD.

Summary points

- Novel mmRNA-loaded nanofibrillar scaffold was developed in our study.
- The scaffold enabled localized, prolonged release of HGF-encoding mmRNA.
- The HGF-encoding mmRNA loaded in scaffold was capable of transfecting seeded human cells *in vitro*.
- The HGF-encoding mmRNA scaffolds was implanted into pig hind leg to bridge ligated femoral artery as a model of peripheral arterial disease.
- Postsurgery computed tomography angiography revealed improved vasculature in scaffold group.
- Histological analysis of microvasculature density within vicinity of the scaffolds suggested the formation of neovessels around the scaffold.
- The scaffold demonstrates its therapeutic efficacy in the porcine model of peripheral arterial disease.

Ethical conduct of research

This study involves conducting surgery and euthanasia on six Yorkshire pigs. Power analysis was performed to minimize the number of animals used to meet our research goal. All animal experiments were performed with approval by the Institutional Animal Care and Use Committee at the Sutter Institute of Medical Research.

References

1. Farber A, Eberhardt RT. The current state of critical limb ischemia: a systematic review. *JAMA Surg.* 151(11), 1070–1077 (2016).

2. Varu VN, Hogg ME, Kibbe MR. Critical limb ischemia. *J. Vasc. Surg.* 51(1), 230–241 (2010).

3. Inampudi C, Akintoye E, Ando T, Briasoulis A. Angiogenesis in peripheral arterial disease. *Curr. Opin. Pharmacol.* 39, 60–67 (2018).

4. Yla-Herttuala S, Rissanen TT, Vajanto I, Hartikainen J. Vascular endothelial growth factors: biology and current status of clinical applications in cardiovascular medicine. *J. Am. Coll. Cardiol.* 49(10), 1015–1026 (2007).

5. Gorenoi V, Brehm MU, Koch A, Hagen A. Growth factors for angiogenesis in peripheral arterial disease. *Cochrane Database Syst. Rev.* 6, CD011741 (2017).

6. Munoz Ruiz M, Regueiro JR. New tools in regenerative medicine: gene therapy. *Adv. Exp. Med. Biol.* 741, 254–275 (2012).

7. Finer M, Glorioso J. A brief account of viral vectors and their promise for gene therapy. *Gene Ther.* 24(1), 1–2 (2017).

8. Hardee CL, Arévalo-Soliz LM, Hornstein BD, Zechiedrich L. Advances in non-viral DNA vectors for gene therapy. *Genes* 8(2), 65 (2017).

9. Chandler RJ, Sands MS, Venditti CP. Recombinant adeno-associated viral integration and genotoxicity: insights from animal models. *Hum. Gene Ther.* 28(4), 314–322 (2017).

10. Van Craenenbroeck K, Vanhoenacker P, Haegeman G. Episomal vectors for gene expression in mammalian cells. *Eur. J. Biochem.* 267(18), 5665–5678 (2000).

11. Cheng L, Hansen NF, Zhao L *et al.* Low incidence of DNA sequence variation in human induced pluripotent stem cells generated by nonintegrating plasmid expression. *Cell Stem Cell* 10(3), 337–344 (2012).

12. Sridharan K, Gogtay NJ. Therapeutic nucleic acids: current clinical status. *Br. J. Clin. Pharmacol.* 82(3), 659–672 (2016).

13. Kariko K, Muramatsu H, Ludwig J, Weissman D. Generating the optimal mRNA for therapy: HPLC purification eliminates immune activation and improves translation of nucleoside-modified, protein-encoding mRNA. *Nucleic Acids Res.* 39(21), e142 (2011).

14. Kormann MS, Hasenpusch G, Aneja MK *et al.* Expression of therapeutic proteins after delivery of chemically modified mRNA in mice. *Nat. Biotechnol.* 29(2), 154–157 (2011).

15. Yu J, Vodyanik MA, Smuga-Otto K *et al.* Induced pluripotent stem cell lines derived from human somatic cells. *Science* 318(5858), 1917–1920 (2007).

16. Okita K, Nakagawa M, Hyenjong H, Ichisaka T, Yamanaka S. Generation of mouse induced pluripotent stem cells without viral vectors. *Science* 322(5903), 949–953 (2008).

17. Kowalski PS, Rudra A, Miao L, Anderson DG. Delivering the messenger: advances in technologies for therapeutic mRNA Delivery. *Mol. Ther.* 27(4), 710–728 (2019).

18. Van Tendeloo VF, Ponsaerts P, Berneman ZN. mRNA-based gene transfer as a tool for gene and cell therapy. *Curr. Opin. Mol. Ther.* 9(5), 423–431 (2007).

19. Schlaeger TM, Daheron L, Brickler TR *et al.* A comparison of non-integrating reprogramming methods. *Nat. Biotechnol.* 33(1), 58–63 (2015).

20. Yamamoto A, Kormann M, Rosenecker J, Rudolph C. Current prospects for mRNA gene delivery. *Eur. J. Pharm. Biopharm.* 71(3), 484–489 (2009).

21. Yakubov E, Rechavi G, Rozenblatt S, Givol D. Reprogramming of human fibroblasts to pluripotent stem cells using mRNA of four transcription factors. *Biochem. Biophys. Res. Commun.* 394(1), 189–193 (2010).

22. Kauffman KJ, Dorkin JR, Yang JH *et al.* Optimization of lipid nanoparticle formulations for mRNA delivery *in vivo* with fractional factorial and definitive screening designs. *Nano Lett.* 15(11), 7300–7306 (2015).

23. Ramunas J, Yakubov E, Brady JJ *et al.* Transient delivery of modified mRNA encoding TERT rapidly extends telomeres in human cells. *FASEB J.* 29(5), 1930–1939 (2015).

24. Wang Y, Su HH, Yang Y *et al.* Systemic delivery of modified mRNA encoding herpes simplex virus 1 thymidine kinase for targeted cancer gene therapy. *Mol. Ther.* 21(2), 358–367 (2013).

25. Kariko K, Muramatsu H, Keller JM, Weissman D. Increased erythropoiesis in mice injected with submicrogram quantities of pseudouridine-containing mRNA encoding erythropoietin. *Mol. Ther.* 20(5), 948–953 (2012).

26. Zangi L, Lui KO, Von Gise A *et al.* Modified mRNA directs the fate of heart progenitor cells and induces vascular regeneration after myocardial infarction. *Nat. Biotechnol.* 31(10), 898–907 (2013).

27. Kariko K, Muramatsu H, Welsh FA *et al.* Incorporation of pseudouridine into mRNA yields superior nonimmunogenic vector with increased translational capacity and biological stability. *Mol. Ther.* 16(11), 1833–1840 (2008).

28. Groth K, Berezhanskyy T, Aneja MK *et al.* Tendon healing induced by chemically modified mRNAs. *Eur. Cell. Mater.* 33, 294–307 (2017).

29. Sultana N, Magadum A, Hadas Y *et al.* Optimizing cardiac delivery of modified mRNA. *Mol. Ther.* 25(6), 1306–1315 (2017).

30. Andre FM, Cournil-Henrionnet C, Vernerey D, Opolon P, Mir LM. Variability of naked DNA expression after direct local injection: the influence of the injection speed. *Gene Ther.* 13(23), 1619–1627 (2006).

31. Wolff JA, Malone RW, Williams P *et al.* Direct gene transfer into mouse muscle *in vivo*. *Science* 247(4949 Pt 1), 1465–1468 (1990).

32. Pardi N, Tuyishime S, Muramatsu H *et al.* Expression kinetics of nucleoside-modified mRNA delivered in lipid nanoparticles to mice by various routes. *J. Control. Release* 217, 345–351 (2015).

33. Jang JH, Rives CB, Shea LD. Plasmid delivery *in vivo* from porous tissue-engineering scaffolds: transgene expression and cellular transfection. *Mol. Ther.* 12(3), 475–483 (2005).

34. Holladay C, Keeney M, Greiser U, Murphy M, O'brien T, Pandit A. A matrix reservoir for improved control of non-viral gene delivery. *J. Control. Release* 136(3), 220–225 (2009).

35. Berry M, Gonzalez AM, Clarke W *et al.* Sustained effects of gene-activated matrices after CNS injury. *Mol. Cell. Neurosci.* 17(4), 706–716 (2001).

36. Balmayor ER, Geiger JP, Koch C *et al.* Modified mRNA for BMP-2 in combination with biomaterials serves as a transcript-activated matrix for effectively inducing osteogenic pathways in stem cells. *Stem Cells Dev.* 26(1), 25–34 (2017).

37. Elangovan S, Khorsand B, Do AV *et al.* Chemically modified RNA activated matrices enhance bone regeneration. *J. Control. Release* 218, 22–28 (2015).

38. Badieyan ZS, Berezhanskyy T, Utzinger M *et al.* Transcript-activated collagen matrix as sustained mRNA delivery system for bone regeneration. *J. Control. Release* 239, 137–148 (2016).

39. Leppanen P, Kholova I, Mahonen AJ *et al.* Short and long-term effects of hVEGF-A(165) in cre-activated transgenic mice. *PLoS ONE* 1, e13 (2006).

40. Kim DH, Provenzano PP, Smith CL, Levchenko A. Matrix nanotopography as a regulator of cell function. *J. Cell Biol.* 197(3), 351–360 (2012).

41. Lai ES, Huang NF, Cooke JP, Fuller GG. Aligned nanofibrillar collagen regulates endothelial organization and migration. *Regen. Med.* 7(5), 649–661 (2012).

42. Wu H, Fan J, Chu CC, Wu J. Electrospinning of small diameter 3-D nanofibrous tubular scaffolds with controllable nanofiber orientations for vascular grafts. *J. Mater. Sci. Mater. Med.* 21(12), 3207–3215 (2010).

43. Ma Z, He W, Yong T, Ramakrishna S. Grafting of gelatin on electrospun poly(caprolactone) nanofibers to improve endothelial cell spreading and proliferation and to control cell orientation. *Tissue Eng.* 11(7–8), 1149–1158 (2005).

44. Huang NF, Lai ES, Ribeiro AJ *et al.* Spatial patterning of endothelium modulates cell morphology, adhesiveness and transcriptional signature. *Biomaterials* 34(12), 2928–2937 (2013).

45. Huang NF, Okogbaa J, Lee JC *et al.* The modulation of endothelial cell morphology, function, and survival using anisotropic nanofibrillar collagen scaffolds. *Biomaterials* 34(16), 4038–4047 (2013).

46. Yang J, Mcnamara LE, Gadegaard N *et al.* Nanotopographical induction of osteogenesis through adhesion, bone morphogenic protein cosignaling, and regulation of microRNAs. *ACS Nano* 8(10), 9941–9953 (2014).

47. Downing TL, Soto J, Morez C *et al.* Biophysical regulation of epigenetic state and cell reprogramming. *Nat. Mater.* 12(12), 1154–1162 (2013).

48. Huang NF, Patel S, Thakar RG *et al.* Myotube assembly on nanofibrous and micropatterned polymers. *Nano Lett.* 6(3), 537–542 (2006).

49. Huang NF, Okogbaa J, Lee JC *et al.* The modulation of endothelial cell morphology, function, and survival using anisotropic nanofibrillar collagen scaffolds. *Biomaterials* 34(16), 4038–4047 (2013).

50. Nakayama KH, Hong G, Lee JC *et al.* Aligned-braided nanofibrillar scaffold with endothelial cells enhances arteriogenesis. *ACS Nano* 9(7), 6900–6908 (2015).

51. Hadamitzky C, Zaitseva TS, Bazalova-Carter M *et al.* Aligned nanofibrillar collagen scaffolds - guiding lymphangiogenesis for treatment of acquired lymphedema. *Biomaterials* 102, 259–267 (2016).

52. Zaitseva TS, Alcazar C, Zamani M *et al.* Aligned nanofibrillar scaffolds for controlled delivery of modified mRNA. *Tissue Eng. Part A* 25(1–2), 121–130 (2019).

53. Stacy MR, Yu DY, Maxfield MW *et al.* Multimodality imaging approach for serial assessment of regional changes in lower extremity arteriogenesis and tissue perfusion in a porcine model of peripheral arterial disease. *Circ. Cardiovasc. Imaging* 7(1), 92–99 (2014).

54. Chung HJ, Kim JT, Kim HJ *et al.* Epicardial delivery of VEGF and cardiac stem cells guided by 3-dimensional PLLA mat enhancing cardiac regeneration and angiogenesis in acute myocardial infarction. *J. Control. Release* 205, 218–230 (2015).

55.   Ochiya T, Takahama Y, Nagahara S *et al.* New delivery system for plasmid DNA *in vivo* using atelocollagen as a carrier material: the minipellet. *Nat. Med.* 5(6), 707–710 (1999).

56.   Carlsson L, Clarke JC, Yen C *et al.* Biocompatible, purified VEGF-A mRNA improves cardiac function after intracardiac injection 1 week post-myocardial infarction in swine. *Mol. Ther. Methods Clin. Dev.* 9, 330–346 (2018).

57.   Turnbull IC, Eltoukhy AA, Fish KM *et al.* Myocardial delivery of lipidoid nanoparticle carrying modRNA induces rapid and transient expression. *Mol. Ther.* 24(1), 66–75 (2016).

58.   Sun N, Ning B, Hansson KM *et al.* Modified VEGF-A mRNA induces sustained multifaceted microvascular response and accelerates diabetic wound healing. *Sci. Rep.* 8(1), 17509 (2018).

59.   De Laporte L, Shea LD. Matrices and scaffolds for DNA delivery in tissue engineering. *Adv. Drug Deliv. Rev.* 59(4–5), 292–307 (2007).

60.   Jang JH, Bengali Z, Houchin TL, Shea LD. Surface adsorption of DNA to tissue engineering scaffolds for efficient gene delivery. *J. Biomed. Mater. Res. Part A* 77(1), 50–58 (2006).

61.   Houchin-Ray T, Swift LA, Jang JH, Shea LD. Patterned PLG substrates for localized DNA delivery and directed neurite extension. *Biomaterials* 28(16), 2603–2611 (2007).

62.   Carlson BM. *Human Embryology and Developmental Biology* (2nd Edition). Mosby, Maryland Heights, MO, USA (1999).

63.   Bengali Z, Rea JC, Shea LD. Gene expression and internalization following vector adsorption to immobilized proteins: dependence on protein identity and density. *J. Gene Med.* 9(8), 668–678 (2007).

64.   Kao WJ. Evaluation of protein-modulated macrophage behavior on biomaterials: designing biomimetic materials for cellular engineering. *Biomaterials* 20(23–24), 2213–2221 (1999).

65.   Gao Y, Aravind S, Patel NS *et al.* Collateral development and arteriogenesis in hindlimbs of swine after ligation of arterial inflow. *J. Surg. Res.* 249, 168–179 (2020).